

Original Research Paper

Advanced XFEM Simulation of Pull-out and Debonding of Steel Bars and FRP-Reinforcements in Concrete Beams

Nicola Orlando and Elena Benvenuti

Department of Engineering, University of Ferrara, I-44122, Ferrara, Italy

Article history

Received: 12-09-2016

Revised: 4-10-2016

Accepted: 5-10-2016

Corresponding Author:

Nicola Orlando

Department of Engineering,

Institute/Organization:

University of Ferrara, I-44122,
Ferrara, Italy

Email: rlnocl@unife.it

Abstract: An innovative three-dimensional model is applied to the pull-out of steel bars and the debonding of FRP plates from concrete specimens. The shearing and opening modes at the interface of debonding is fully captured. The model is based on an innovative variant of the regularized eXtended Finite Element Method (XFEM) developed by the authors. In this method, the displacement discontinuity at the debonding surface is regularized and an internal length parameter is introduced. Besides smoothing the debonding, the regularized XFEM is particularly suitable for modelling steel fiber reinforced beams.

Keywords: Pull-Out, Debonding, XFEM, Bending Test, 3D, Mixed-Mode

Introduction

In this study, an innovative three-dimensional (3D) approach for modelling the bond behavior of steel bars embedded in concrete blocks and FRP plates glued to concrete beams is presented. The approach adopted is based on a recently developed procedure called regularized eXtended Finite Element Method (regularized XFEM) Benvenuti *et al.* (2016), that extends a previous two-dimensional (2D) formulation for cohesive-like interfaces, Benvenuti *et al.* (2012), Benvenuti *et al.* (2013).

The regularized XFEM is a variant of the eXtended Finite Element Method developed by Belytschko *et al.* (2009), Moës *et al.* (1999). Recent applications of XFEM in civil engineering can be found in Jaśkowiec (2015) and in Huo *et al.* (2015). However, the applications of XFEM to the simulation of the debonding of FRP plates from concrete beams subjected to bending are rather few. An example is the work by Dror and Rabinovitch (2016).

In the approach proposed in the present paper, the displacement discontinuities are regularized introducing an additional internal length parameter. Moreover, a suitable variational formulation is adopted, based on the concept of Eshelby's equivalent eigenstrain Eshelby (1957), as shown in Benvenuti (2014). A wide range of loading cases and types of reinforcement is considered to prove the generality and the reliability of the present approach. In particular, the following experimental tests have been modelled:

- Pull-out test of steel bars embedded in concrete blocks
- Three point bending tests of Steel-Fibers Reinforced Concrete (SFRC) beams strengthened with flexural FRP reinforcements
- Four point bending test of steel Reinforced Concrete (RC) beams strengthened with flexural FRP reinforcements

The detachment of FRP plates from supports made of quasi-brittle materials is commonly modelled as 2D plane stress problems replacing the FRP-concrete cover with an equivalent non-linear one-dimensional bond stress-slip law. Relevant applications to FRP-reinforced concrete blocks subjected to shear tests can be found in Turon *et al.* (2007) and Toti *et al.* (2013).

It has been demonstrated in Czaderski *et al.* (2010), Martinelli *et al.* (2011), Subramaniam *et al.* (2011), that the detachment of FRP reinforcement from concrete supports involves the development of a 3D strain/stress distribution and occurs in a mixed debonding mode. These aspects cannot be captured using 2D models that account for the only shear debonding mechanisms. 3D effects have been studied by Neto *et al.* (2014).

The presented approach takes into account both the mixed mode debonding and 3D effects.

The latter aspect has been discussed in Benvenuti *et al.* (2016) for the case of single-lap shear tests. In this study, the focus is on the former aspect, namely on the mixed-mode debonding.

Main Features of the Regularized XFEM

The proposed approach models the mechanical behavior of displacement discontinuities in brittle materials. A briefly review of the approach has been reported hereinafter. More details about the proposed approach can be found in Benvenuti (2014), Benvenuti *et al.* (2016).

An additional internal length governing the width of the process zone is introduced. The adopted regularization avoids the possible mesh-dependency induced by softening damaging laws. Moreover, a smooth continuous-discontinuous transition is obtained, Benvenuti and Tralli (2012). The approach is based on a damage procedure that can correctly reproduce mixed-mode debonding, as shown in the single-lap shear tests previously presented.

Let the displacement field \mathbf{u} be discontinuous across the failure surface defined according the mechanical problem $S \in \mathbf{R}^3$ of normal \mathbf{n}_S . Within a single element of nodal degrees of freedom \mathbf{U}^e and \mathbf{A}^e interpolated by the usual FE interpolation functions \mathbf{N}^e , the regularized XFEM displacement \mathbf{u}^e of element e is:

$$\mathbf{u}^e = \mathbf{N}^e \mathbf{U}^e + H_\rho \mathbf{N}^e \mathbf{A}^e, \quad (1)$$

where, H_ρ is the regularized Heaviside function (Fig. 1). This regularized function approximates the Heaviside function for vanishing regularization parameter ρ . The vector \mathbf{A}^e collects the jump components along x , y and z for the finite element e . H_ρ is assumed a function of the signed distance from the level-set surface. By compatibility, the strain field is:

$$\boldsymbol{\varepsilon}^e = \boldsymbol{\varepsilon} + \boldsymbol{\varepsilon}_\rho + \boldsymbol{\delta}_\rho, \quad (2)$$

$$\boldsymbol{\varepsilon} = \mathbf{B}^e \mathbf{U}, \quad (2a)$$

$$\boldsymbol{\varepsilon}_\rho = H_\rho \mathbf{B}^e \mathbf{A}^e \quad (2b)$$

$$\boldsymbol{\delta}_\rho = \gamma_\rho (\mathbf{N}^e \mathbf{A}^e \otimes \mathbf{n}_S), \quad (2c)$$

where, $\mathbf{B}^e = \nabla \mathbf{N}^e$ is the standard FE compatibility matrix and $\gamma_\rho = \|\nabla H_\rho\|$ (implying that $\nabla H_\rho = \|\nabla H_\rho\| \mathbf{n}_S = \gamma_\rho \mathbf{n}_S$).

Strains $\boldsymbol{\varepsilon}$ and $\boldsymbol{\varepsilon}_\rho$ represent respectively the deformation of the bulk in absence of regularized and the spatial variation of the discontinuity intensity \mathbf{A}^e . Strain $\boldsymbol{\delta}_\rho$ corresponds to the strain localized over the regularization volume V_ρ . Steel bars, FRP plates and adhesive layers are usually modelled as linear elastic materials. At each Gauss point, the damage variables D and D_c for the concrete are introduced. Then, with $\mathbf{E}_c = \mathbf{E} / \gamma_\rho$, the stresses are computed as:

$$\boldsymbol{\sigma}^e = (1 - D) \mathbf{E} \boldsymbol{\varepsilon} + (1 - D) \mathbf{E} \boldsymbol{\varepsilon}_\rho, \quad (3)$$

$$\boldsymbol{\sigma}_c^e = (1 - D_c) \mathbf{E}^c \boldsymbol{\delta}_\rho. \quad (4)$$

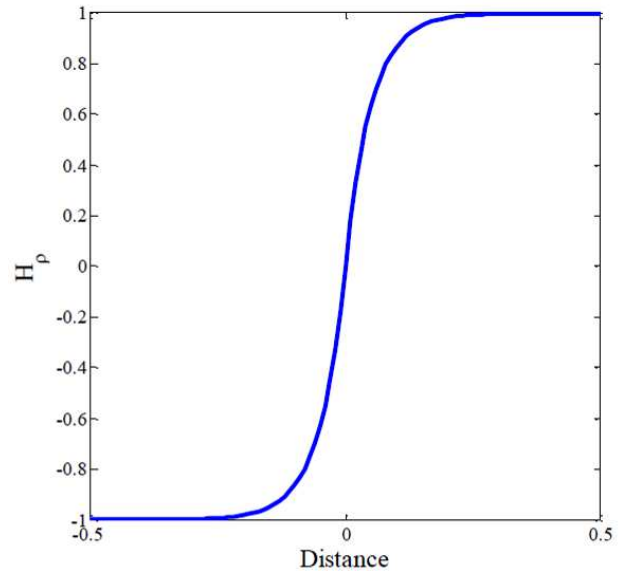


Fig. 1. Regularized Heaviside function

The stress $\boldsymbol{\sigma}^e$ pertains to the bulk material and is governed by the constitutive matrix \mathbf{E} and the damage variable D . In particular, the damage D ranges from 0 (material sound) up to the critical value D_{cr} , when the evolution of damage of D is dropped. D is governed by the Galileo-Rankine criterion:

$$\begin{aligned} \boldsymbol{\sigma} &= \mathbf{E} \boldsymbol{\varepsilon}, \\ \bar{\boldsymbol{\sigma}} &= \max \{ \sigma_1, \sigma_2, \sigma_3 \}. \end{aligned} \quad (5)$$

The exponential elasto-damaging law (Fig. 2) is assumed:

$$\begin{aligned} \text{If } \bar{\boldsymbol{\sigma}} &\geq f_t, \\ D &= \min \left\{ D_{cr}, 1 - \frac{f_t}{\bar{\boldsymbol{\sigma}}} \exp \left(-2H \frac{\bar{\boldsymbol{\sigma}} - f_t}{f_t} \right) \right\}, \end{aligned} \quad (6)$$

where, $H \geq 0$ is a softening parameter and f_t is the tensile strength of the concrete.

The function γ_ρ has a non-compact support. The contribution of points whose distance is larger than 20ρ from the discontinuity surface is neglected.

As soon as the damage D reaches the critical value D_{cr} in an element inside the regularization volume of height 40ρ centered on the crack, the regularization is activated for the element. In particular, two cases can occur:

- The size of the mesh is smaller than the value of 40ρ , which leads to a *thick process zone*
- The size of the mesh is larger than the value of 40ρ , which leads to a *thin process zone*

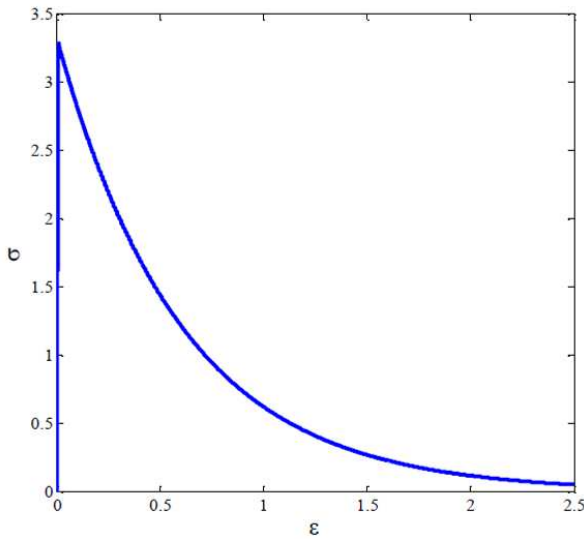


Fig. 2. Exponential Rankine elasto-damaging law adopted

When the regularization is activated, the evolution of damage in the element is linked to the variable D_c . The scalar equivalent stress $\bar{\sigma}^c$ related to the evolution of D_c is computed as:

$$\sigma^c = \begin{cases} \mathbf{E}^c \delta_\rho \text{ case of thin process zone} \\ \gamma_\rho \mathbf{E}^c \delta_\rho \text{ case of thick process zone} \end{cases} \quad (7)$$

$$\bar{\sigma}^c = \max\{\sigma_1^c, \sigma_2^c, \sigma_3^c\},$$

The damage D_c is governed by the same softening law used for the bulk:

if $\bar{\sigma}^c \geq f_t$,

$$D_c = \max\left\{D_{cr}, 1 - \frac{f_t}{\bar{\sigma}^c} \exp\left(-2H \frac{\bar{\sigma}^c - f_t}{f_t}\right)\right\} \quad (8)$$

The mixed-mode debonding is modelled through the adoption of a local level-set defined at the Gauss point level. In the constitutive model, \mathbf{n}_s represents the normal unit vector of the discontinuity surface. The damage D_c is affected by \mathbf{n}_s . While for mode I discontinuities \mathbf{n}_s has to be orthogonal to the surface discontinuity, it has been found that for describing mixed-mode debonding a different orientation of the vector is required.

Let us imagine that the regularized layer can be regarded as a series of inclined trusses as shown in Fig. 3. For the mixed loading mode of Fig. 3, the vector \mathbf{n}_s has to be aligned along the direction of the trusses in the deformed configuration. Noteworthy, the local level-set is imposed a priori, but the final directions of the jump vectors \mathbf{A}^c at the nodes are computed by the nonlinear iterative-incremental procedure and will not generally coincide with that of the superimposed \mathbf{n}_s .

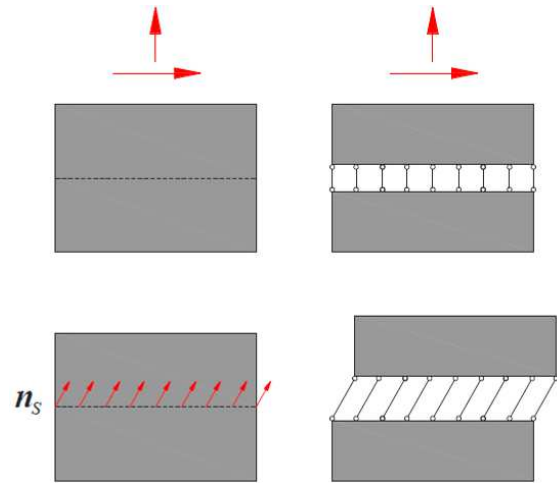


Fig. 3. Example of local level-set for mixed-mode debonding. The mechanical behaviour of the discontinuity surface is schematized with the trusses

In the numerical results shown in the forthcoming sections, tetrahedral elements have been used.

Pull-Out

In this section, the pull-out test on a steel rebar embedded in a concrete block has been investigated by means of the proposed regularized XFEM approach. As reference results, the experimental findings of Xiao and Falkne (2007) have been considered, where two sets of pull-out tests were performed using plain and deformed bars for the specimens shown in Fig. 4.

The mechanical properties of the concrete are: compressive strength $f_{cu} = 43.52 \text{ MPa}$, Young's modulus $E_c = 34.2 \text{ GPa}$ and Poisson ratio $\nu = 0.2$. The plain and the deformed steel rebars have Young's modulus $E_c = 210 \text{ GPa}$, Poisson ratio $\nu = 0.3$ and respectively a yield strength equals to $f_{yk} = 300 \text{ MPa}$ and $f_{yk} = 420 \text{ MPa}$. The load was applied by a testing machine to the end of the rebar, while the slip at the free end of the rebar was recorded.

In the simulations, the material parameters of the damage law have been calibrated. In particular, for the plain bar $f_t = 7.0 \text{ MPa}$ and $H = 2.5 \cdot 10^{-5}$ have been used, while, for the deformed bar, $f_t = 13.5 \text{ MPa}$ and $H = 1.0 \cdot 10^{-4}$ have been imposed. For both the applications, the regularization parameter have been set to $\rho = 0.0250 \text{ mm}$, enriching only one layer of finite elements having mesh size $h = 1 \text{ mm}$ (thin process zone). The threshold value of damage D_{cr} have been set to $D_{cr} = 0.001$. In this way, the damaging process occurs in the enriched elements.

The numerical and the experimental results are compared in Fig. 5, where the grey zone with the dashed profiles indicates the experimental results. To reduce the computational burden, only a quarter of the specimen have been meshed (Fig. 6).

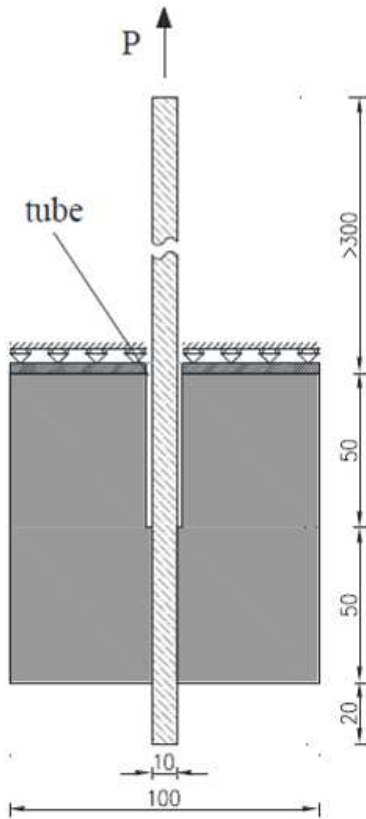


Fig. 4. Pull-out: Geometries of the Xiao and Falkne (2007) specimen (dimensions in mm)

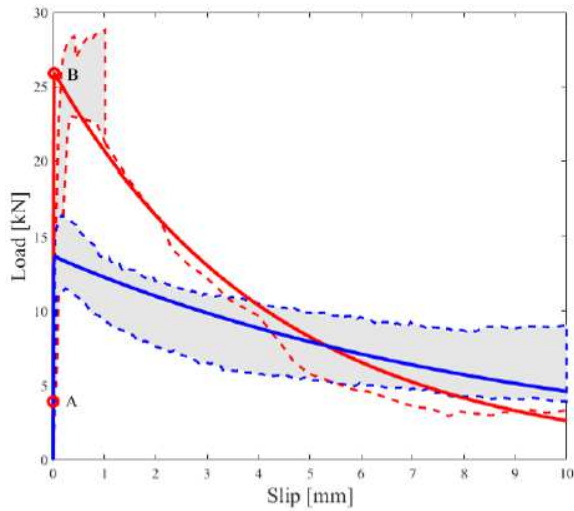


Fig. 5. Pull-out: Computed (continuous lines) and experimental (grey areas) load-slip profiles for plain bars (blue lines) and deformed bars (red lines) (see Fig. 7 for the contour plots of damage)

The contour plots of the damage evolution of the concrete specimen during the load process for the deformed bar have been reported in Fig. 7.

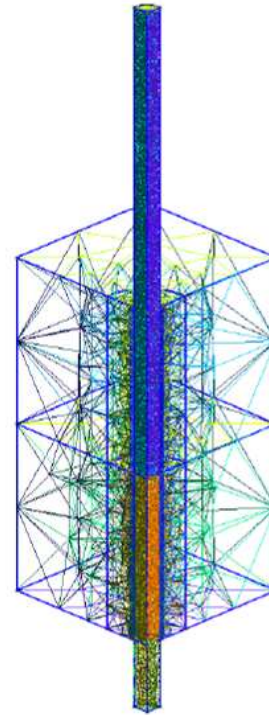


Fig. 6. Pull-out: Mesh of a quarter of pull-out specimen having 22662 dofs and minimum mesh size $h=1\text{ mm}$

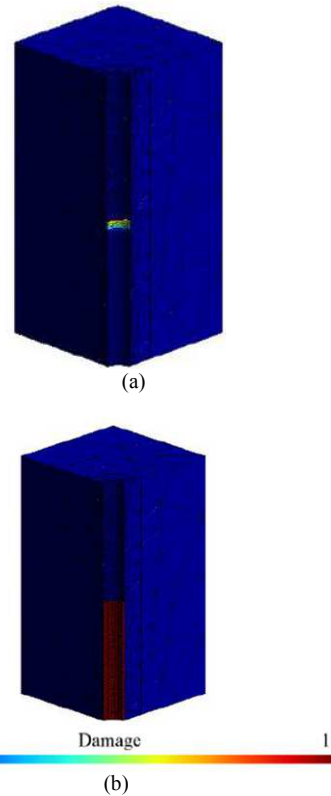


Fig. 7. Pull-out: Evolution of Damage during the load process (see Fig. 5) (a) Step A (b) Step B

It is clear that the damage starts to develop from the loaded end and propagates towards the free ends of the bar. The peak load is reached when the whole bond surface is damaged.

The agreement between the computed and the experimental load displacement results is very satisfying for the entire load process.

FRP Flexural Strengthening

This section is devoted to investigate the debonding of FRP flexural reinforcements from concrete beams using the regularized XFEM approach.

Several studies on FRP strengthening technique are available, such as Turon *et al.* (2007), Carrara *et al.* (2011), Toti *et al.* (2013), Carrara and Ferretti (2013), Neto *et al.* (2014). It has been proved that the debonding occurs within the concrete layer few millimeters beneath the adhesive layer. In particular, the following debonding modes (see Fig. 8) in bending, Smith and Teng (2002), Aram *et al.* (2008), test have been identified:

- Plate end debonding
- Debonding by flexural cracks
- Debonding by shear cracks

In the present study, two different experimental campaigns have been modelled.

Three Point Bending Test

As a first case-study, the experimental program carried out by Yin and Wu (2003) on Steel Fiber Reinforced Concrete beams (SFRC) has been modeled. In their study, the concrete beam strengthened with a FRP flexural reinforcement shown in Fig. 9 was subjected to a three point bending test. A concrete with compressive strength $f_{cm} = 26 \text{ MPa}$, Young's modulus $E_c = 25 \text{ GPa}$ and Poisson ratio $\nu = 0.2$ was employed.

No standard steel reinforcement bars were employed. Short steel-fibers of length $l_f = 30 \text{ mm}$ and diameter $\varnothing_f = 0.5 \text{ mm}$ were added to the concrete mixture. In the present simulations, three different mixtures of SFRC, with fiber volume fraction $V_f = 0\%, 0.25\%, 1.0\%$ respectively, have been considered. To relate the tensile strength of the concrete to V_f , the Job and Ananth (2007) formula:

$$f_{spc} = 0.63(f_{cm})^{0.5} + 0.288(f_{cm})^{0.5} RI + 0.052RI \quad (8)$$

has been adopted. In Equation 8, $RI = V_f l_f / \varphi_f$ is the fiber reinforced index. The value of the softening parameter has been kept constant to $H = 0.008$ for all the applications.

The steel-fibers act as a diffuse reinforcement system. Debonding and pulling out of fibers during the cracking development dissipate energy, implying a substantial increase in toughness and strength for growing V_f .

In the proposed regularized XFEM approach, the dissipation of the energy at the debonding surface material is influenced by the regularization parameter ρ . In particular, the bigger ρ the higher the peak load of the load-displacement profiles. Moreover, the presence of ρ prevents the sudden loss of stiffness at the surface of the FRP debonding. A posteriori, the following linear relationship between the volume fraction V_f and the regularization parameters ρ .

$$\rho = 0.1875 (1 + V_f), \quad (9)$$

has been identified.

In these simulations, the damage threshold D_{cr} has been set to $D_{cr} = 0.995$. This choice allows the correct development of the cracks into the bulk before the activation of the continuous-discontinuous transition.

The comparison between numerical and experimental results are shown in Fig. 11. Exploiting the double symmetry of the test, only a quarter of the specimen have been modelled (Fig. 10).

As found in the experiments, in the numerical simulations, the FRP debonding (see Fig. 16) is triggered by the concentration of the interfacial shear stress near a flexural/shear crack after the occurrence of diffused flexural cracks in the concrete. Then, the debonding propagates towards the plate ends.

Furthermore, the computed loads at the crack initiation and at the debonding initiation are very similar to the experimental values recorded by Yin and Wu (2003).

The experimental failure modes are correctly predicted with the thick zone process. Moreover, the agreement between experimental and numerical load-deflection results for all the values of fiber volume fraction is highly satisfying.

Four Point Bending Test

As a second application, the experimental setup of Barros *et al.* (2007) has been considered. For this purpose, the concrete beam of Fig. 12 has been considered. For the concrete, the compressive strength $f_{cm} = 44.2 \text{ MPa}$, Young's modulus $E_c = 34.4 \text{ GPa}$ and Poisson's ratio $\nu = 0.2$ was employed. Following Barros *et al.* (2007), the steel bar reinforcements with diameter $\varnothing_s = 6.5 \text{ mm}$, $f_{yk} = 627 \text{ MPa}$ and a $E_s = 210 \text{ GPa}$ have been modeled.

In order to record the enhancement on ultimate load with FRP reinforcement, the beam was subjected to a four point bending test. A control test on a beam without FRP flexural reinforcement was also carried out. The comparison between experimental and numerical data is shown in Fig. 13.

The analyses have been computed taking the tensile strength of the concrete equals to $f_{ct} = 3.28 \text{ MPa}$ and the softening parameter equal to $H = 0.008$.

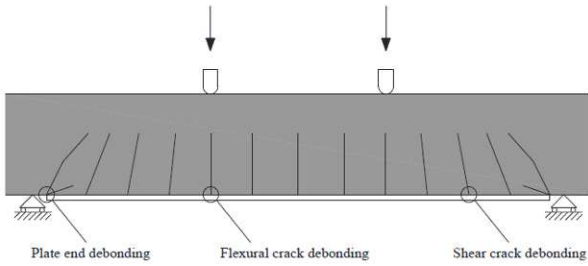


Fig. 8. FRP debonding main failure modes

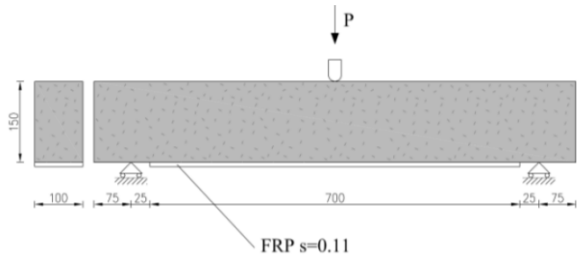


Fig. 9. Three Point Bending Test: Geometry of the specimen (dimensions in "mm")

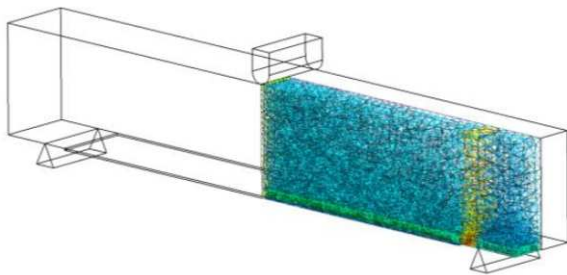


Fig. 10. Three Point Bending Test: Mesh of a quarter of the specimen having 91072 dofs and minimum mesh size $h=5$ "mm"

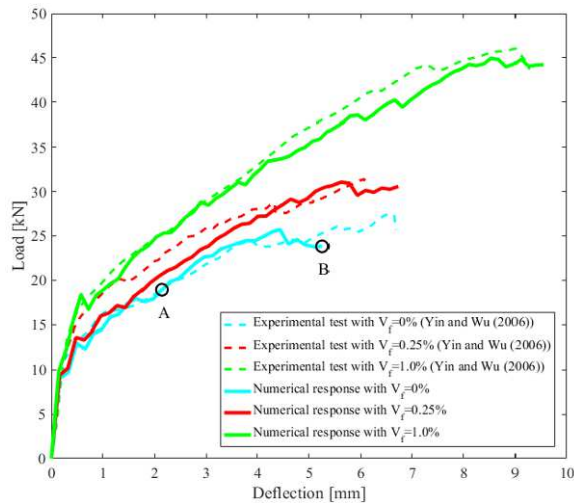


Fig. 11. Three Point Bending Test: and experimental load-deflection profiles (see Fig. 16 for the deformed crack pattern)

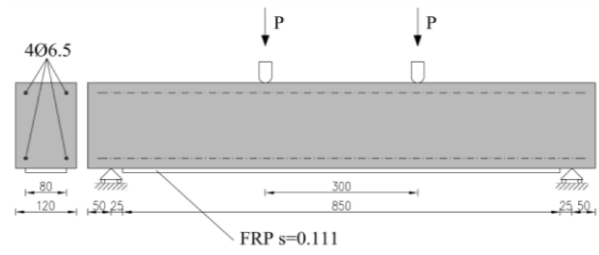


Fig. 12. Four Point Bending Test: Specimen geometries (dimensions in mm)

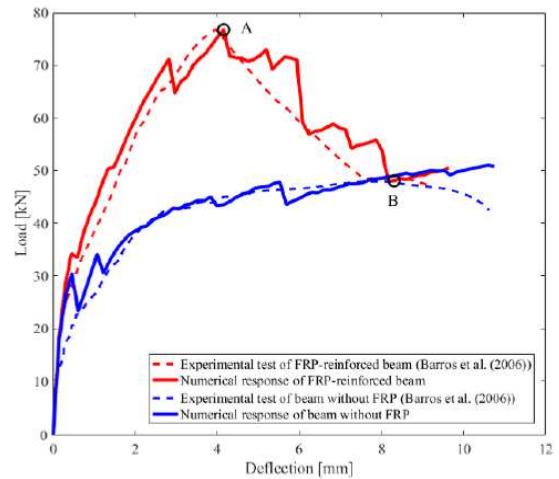


Fig. 13. Four Point Bending Test: Computed and experimental load-deflection (see Fig. 16 for the deformed crack pattern)

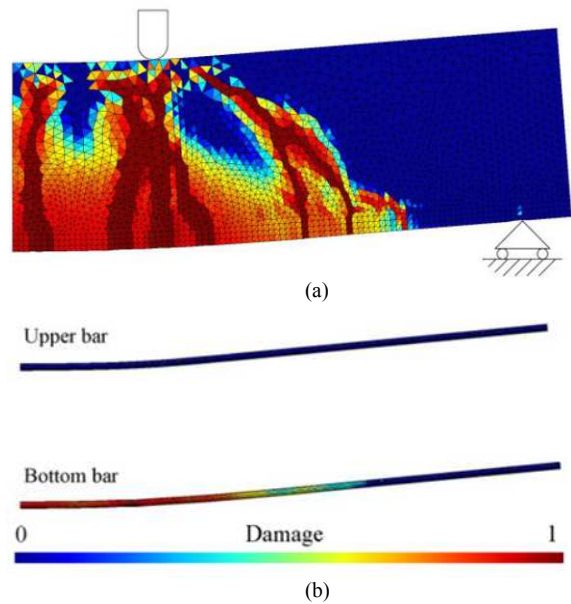


Fig. 14. (a) Deformed (magnification factor 3) crack pattern at failure of the beam without FRP reinforcement. (b) shows the particular of the yielding of the bottom bar

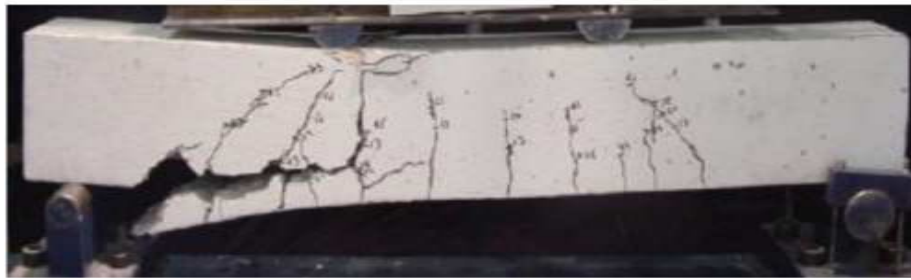


Fig. 15. Pictures of the experimental failure mode obtained by Barros *et al.* (2006)

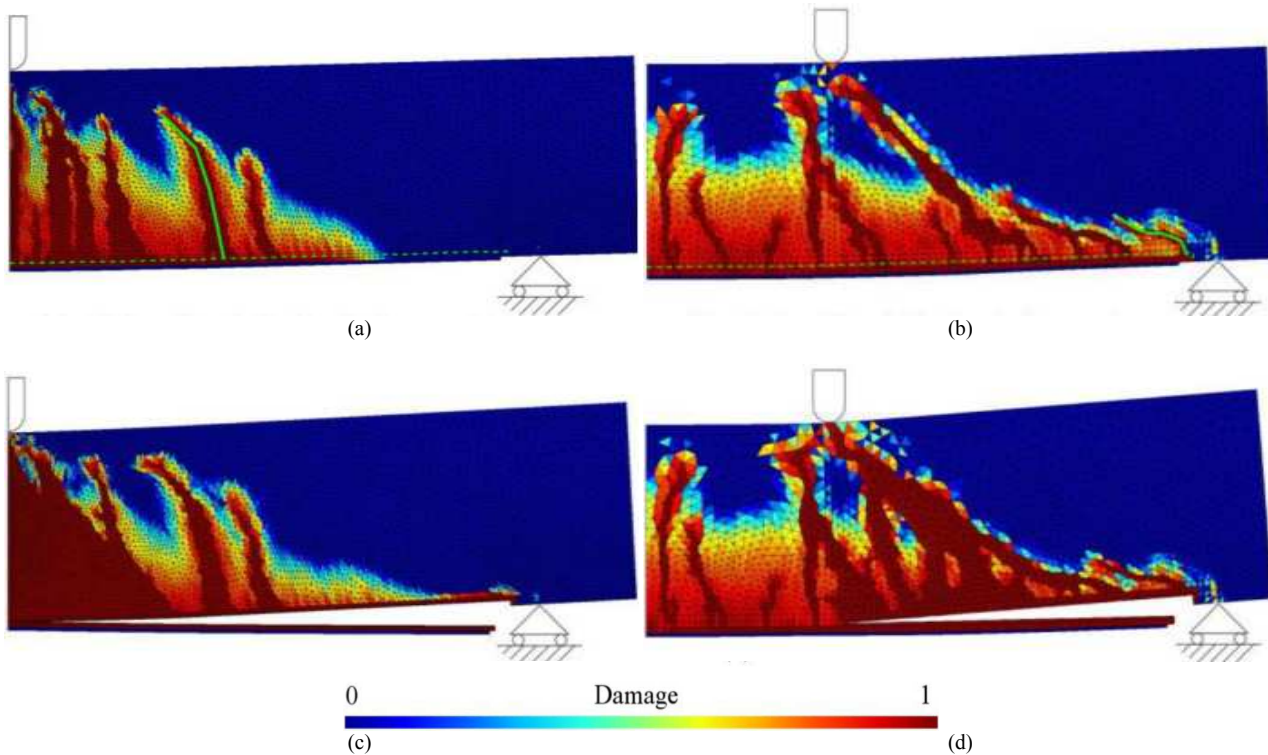


Fig. 16. Comparison of FRP debonding failure modes between three and four point bending test (magnification factor 3). (a) Debonding initiation in three point test (b) Debonding initiation in four point test (c) Debonding failure by shear cracks (d) plate end debonding failure

According to the experimental evidences, such as Smith and Teng (2002), Barros *et al.* (2007), Aram *et al.* (2008), the surface of the debonding has been imposed between concrete cover and steel reinforcement. The regularization parameters has been kept equals to $\rho=0.375 \text{ mm}$ (thick zone process). Only a quarter of the specimen has been meshed to reduce the computational burden of the analyses. A mesh with 130203 dofs and minimum mesh size $h=5\text{mm}$ has been used.

In Fig. 14 the deformed crack pattern at failure of the beam without the FRP reinforcement has been reported. The failure of the beam was due to the yielding of the bottom steel reinforcements at the flexural crack under the load application point.

In Fig. 16 the comparison between the failure modes of the three and four point bending test has been reported. The FRP debonding mode is different from the three point bending test. In the four point test the debonding starts to propagates from the plate end of the sheet. Then the process continues towards the mid-span of the beam, until the complete detachment of the reinforcement. As expected, the load profile after the total debonding follows the structural path of the beam without the FRP reinforcement.

In Fig. 15 a picture of the experimental FRP debonding is shown. It is remarkable that the experimental mode validates the performed analyses. The good agreement between numerical and experimental data is very satisfying.

Conclusion

The regularized 3D XFEM approach has been successfully applied to simulate the pull-out of steel rebars and the debonding of the FRP-plates in pull-out and bending tests. In particular, the numerical simulations have shown that:

- The pull-out of the rebars is correctly captured for both plain and deformed bars, adopting a thin debonding layer of 1 mm
- In the three point bending tests of SFRC beams, the regularization length parameter makes it possible to capture the influence of the fiber volume content on the structural response
- In the simulated three and four point bending tests, the procedure of continuous-discontinuous transition makes the correct development of the debonding behavior possible
- The procedure is able to model 3D mixed debonding mode
- In general, the structural responses obtained agree with the experimental data

These results confirm the reliability of the model, which can be a useful tool together and in alternative to experimental tests.

Acknowledgement

This research was supported by the University of Ferrara.

Author's Contributions

Nicola Orlando: Performed numerical analysis, interpreted data, wrote manuscript and acted as corresponding author.

Elena Benvenuti: Supervised development of work, helped in data interpretation and manuscript evaluation.

References

- Aram, M.R., C. Czaderski and M. Motavalli, 2008. Debonding failure modes of flexural FRP-strengthened RC beams. *Composites part B: Engineering*, 39: 826-841. DOI:10.1016/j.compositesb.2007.10.006
- Barros, J.A., S.J. Dias and J.L. Lima. 2007. Efficacy of CFRP-based techniques for the flexural and shear strengthening of concrete beams. *Cement Concrete Composites*, 29: 203-217. DOI: 10.1016/j.cemconcomp.2006.09.001
- Belytschko, T., R. Gracie and G. Ventura, 2009. A review of extended/generalized finite element methods for material modeling. *Modelling Simulation Materials Sci. Eng.*, 17: 043001.
- Benvenuti, E. and A. Tralli, 2012. Simulation of finite-width process zone in concrete-like materials by means of a regularized extended finite element model. *Computational Mechanics*, 50: 479-497. DOI: 10.1007/s00466-012-0685-y
- Benvenuti, E., 2014. XFEM with equivalent eigenstrain for matrix-inclusion interfaces. *Computational Mechanics*, 53: 893-908. DOI: 10.1007/s00466-013-0938-4
- Benvenuti, E., G. Ventura, N. Ponara and A. Tralli, 2013. Variationally consistent eXtended FE model for 3D planar and curved imperfect interfaces. *Computer Methods Applied Mechanics Eng.*, 267: 434-457. DOI: 10.1016/j.cma.2013.08.013
- Benvenuti, E., N. Orlando, D. Ferretti and A. Tralli, 2016. A new 3D experimentally consistent XFEM to simulate delamination in FRP-reinforced concrete. *Composites Part B: Engineering*, 91: 346-360. DOI: 10.1016/j.compositesb.2016.01.024
- Benvenuti, E., O. Vitarelli and A. Tralli. 2012. Delamination of FRP-reinforced concrete by means of an extended finite element formulation. *Composites Part B: Eng.*, 43: 3258-3269. DOI: 10.1016/j.compositesb.2012.02.035
- Carrara, P. and D. Ferretti, 2013. A finite-difference model with mixed interface laws for shear tests of FRP plates bonded to concrete. *Composites Part B: Engineering*, 54: 329-342. DOI:10.1016/j.compositesb.2013.05.030
- Carrara, P., D. Ferretti, F. Freddi and G. Rosati, 2011. Shear tests of carbon fiber plates bonded to concrete with control of snap-back. *Engineering Fracture Mechanics*, 78: 2663-2678. DOI:10.1016/j.engfracmech.2011.07.003
- Czaderski, C., K. Soudki and M. Motavalli, 2010. Front and side view image correlation measurements on FRP to concrete pull-off bond tests. *J. Composites Construction*, 14: 451-463. DOI: 10.1061/(ASCE)CC.1943-5614.0000106
- Dror, E.B. and O. Rabinovitch, 2016. Size effect in the debonding failure of FRP strengthened beams. *Eng. Fracture Mechanics*, 156: 161-181. DOI: 10.1016/j.engfracmech.2016.02.007
- Eshelby, J.D., 1957. The determination of the elastic field of an ellipsoidal inclusion and related problems. *Proceedings Royal Society London A: Mathematical, Physical Eng. Sci.*, 241: 376-396. DOI: 10.1098/rspa.1957.0133
- Huo, Z.Y., G.X. Qian and D.J. Zheng, 2015. Seepage Analysis of the Structure with Cracks Based on XFEM. *Open Civil Eng. J.*, 9: 90-97. DOI: 10.2174/1874149501509010090

- Jaśkowiec, J., 2015. Numerical modeling mechanical delamination in laminated glass by XFEM. *Procedia Engineering*, 108: 293-300.
DOI: 10.1016/j.proeng.2015.06.150
- Martinelli, E., C. Czaderski and M. Motavalli, 2011. Modeling in-plane and out-of-plane displacement fields in pull-off tests on FRP strips. *Engineering Structures*, 33: 3715-3725.
DOI:10.1016/j.engstruct.2011.08.008
- Moës, N., J. Dolbow and T. Belytschko, 1999. A finite element method for crack growth without remeshing. *Int. J. Numerical Methods Eng.*, 46: 131-150.
- Neto, P., J. Alfaiate and J. Vinagre, 2014. A three-dimensional analysis of CFRP-concrete bond behaviour. *Composites Part B: Eng.*, 59: 153-165.
DOI: 10.1016/j.compositesb.2013.11.025
- Smith, S.T. and J.G. Teng, 2002. FRP-strengthened RC beams. I: review of debonding strength models. *Eng. Structures*, 24: 385-395.
DOI: 10.1016/S0141-0296(01)00105-5
- Subramaniam, K.V., C. Carloni and L. Nobile, 2011. An understanding of the width effect in FRP-concrete debonding. *Strain*, 47: 127-137.
DOI: 10.1111/j.1475-1305.2008.00481.x
- Thomas, J. and A. Ramaswamy, 2007. Mechanical properties of steel fiber-reinforced concrete. *J. Materials Civil Engineering*, 19: 385-392.
DOI: 10.1061/(ASCE)0899-1561(2007)19:5(385)
- Toti, J., S. Marfia and E. Sacco, 2013. Coupled body-interface nonlocal damage model for FRP detachment. *Comput. Methods Applied Mechanics Eng.*, 260: 1-23. DOI: 10.1016/j.cma.2013.03.010
- Turon, A., C.G. Davila, P.P. Camanho and L. Costa, 2007. An engineering solution for mesh size effects in the simulation of delamination using cohesive zone models. *Eng. Fracture Mechanics*, 74: 1665-1682.
DOI: 10.1016/j.engfracmech.2006.08.025
- Xiao, J. and H. Falkner, 2007. Bond behaviour between recycled aggregate concrete and steel rebars. *Construction and Building Materials*, 21: 395-401.
DOI: 10.1016/j.conbuildmat.2005.08.008
- Yin, J., Z.S. Wu, 2003. Structural performances of short steel-fiber reinforced concrete beams with externally bonded FRP sheets. *Construction Building Materials*, 17: 463-470.
DOI: 10.1016/S0950-0618(03)00044-8